Zili Ma, Can Lu, Jianhong Chen, Anna Rokicińska, Piotr Kuśtrowski, Robert Coridan, Richard Dronskowski, Adam Slabon* and Aleksander Jaworski*

$CeTiO_2N$ oxynitride perovskite: paramagnetic ^{14}N MAS NMR without paramagnetic shifts

https://doi.org/10.1515/znb-2021-0031
Received March 9, 2021; accepted March 20, 2021;
published online May 3, 2021

Abstract: ^{14}N magic-angle spinning (MAS) nuclear magnetic resonance (NMR) spectra of diamagnetic $LaTiO_2N$ perovskite oxynitride and its paramagnetic counterpart $CeTiO_2N$ are presented. The latter, to the best of our knowledge, constitutes the first high-resolution ^{14}N MAS NMR spectrum collected from a paramagnetic solid material. The unpaired 4*f*-electrons in $CeTiO_2N$ do not induce a paramagnetic ^{14}N NMR shift. This is remarkable given the direct Ce–N contacts in the structure for which *ab initio* calculations predict substantial Ce→^{14}N contact shift interaction. The same effect is revealed with ^{14}N MAS NMR for $SrWO_2N$ (unpaired 5*d*-electrons).

Keywords: DLPNO-CCSD; lanthanides; ^{14}N MAS NMR; paramagnetic NMR; perovskites.

***Corresponding authors: Adam Slabon and Aleksander Jaworski,** Department of Materials and Environmental Chemistry, Stockholm University, SE-106 91, Stockholm, Sweden,
E-mail: adam.slabon@mmk.su.se (A. Slabon), aleksander.jaworski@mmk.su.se (A. Jaworski), https://orcid.org/0000-0002-4452-1831 (A. Slabon), https://orcid.org/0000-0002-7156-559X (A. Jaworski)
Zili Ma, Can Lu and Richard Dronskowski, Chair of Solid-State and Quantum Chemistry, Institute of Inorganic Chemistry, RWTH Aachen University, Landoltweg 1, D-52056 Aachen, Germany,
E-mail: z.l.ma@qq.com (Z. Ma), can.lu@ac.rwth-aachen.de (C. Lu), drons@HAL9000.ac.rwth-aachen.de (R. Dronskowski). https://orcid.org/0000-0001-7975-9201 (Z. Ma). https://orcid.org/0000-0002-1925-9624 (R. Dronskowski)
Jianhong Chen, Department of Materials and Environmental Chemistry, Stockholm University, SE-106 91, Stockholm, Sweden,
E-mail: jianhong.chen@mmk.su.se
Anna Rokicińska and Piotr Kuśtrowski, Faculty of Chemistry, Jagiellonian University, Gronostajowa 2, 30-387 Kraków, Poland,
E-mail: anna.rokicinska@uj.edu.pl (A. Rokicińska), piotr.kustrowski@uj.edu.pl (P. Kuśtrowski). https://orcid.org/0000-0001-8397-4422 (A. Rokicińska). https://orcid.org/0000-0001-8496-0559 (P. Kuśtrowski)
Robert Coridan, Department of Chemistry and Biochemistry, University of Arkansas, Fayetteville, AR 72701, USA,
E-mail: rcoridan@uark.edu. https://orcid.org/0000-0003-1916-4446

1 Introduction

$LaTiO_2N$ and other oxynitride semiconductors with the perovskite crystal structure exhibit favorable band gaps and visible-light-driven photocatalytic activity for water splitting reactions and hence constitute one of the most promising types of materials for this purpose [1–10]. Local O^{2-}/N^{3-} anion ordering in these systems is predicted to have significant implications on properties such as band gaps and was studied with X-ray, electron, and neutron diffraction, as well as first-principles calculations [11–19]. However, local O^{2-}/N^{3-} ordering occurs on too short length scales to be observed by diffraction techniques [14]. Moreover, O^{2-} and N^{3-} ions differ in charge, ionic radii, and coordination preferences and thus are not expected to occupy the same positions, as they are enforced in structures derived from diffraction measurements, which are biased by averaging. On the other hand, solid-state NMR probes nitrogen atoms directly, regardless of the chemical/structural disorder. Therefore, in this work, we present ^{14}N magic-angle spinning (MAS) NMR spectra of $LaTiO_2N$ and its paramagnetic counterpart $CeTiO_2N$, which may provide further insights into Ce/N/O arrangements in these structures. The paramagnetic nature of $CeTiO_2N$ was revealed by magnetic measurements resulting in a Weiss constant $\theta = -28$ K and effective magnetic moment $\mu_{eff} = 2.43$ [14], in line with that expected for the free Ce^{3+} ion (2.54), in contrast to Ti^{3+} (1.73). To the best of our knowledge, this is the first-reported high-resolution ^{14}N MAS NMR spectrum of a solid paramagnetic material, considering previous attempts performed under static conditions and cryogenic temperatures. Schulman and Wyluda in 1962 reported ^{14}N continuous-wave (dispersion mode) NMR experiments on rare-earth nitrides (cubic structure): TbN and TmN. The observed signals were shifted significantly upfield with respect to the reference (liquid nitrogen) due to the hyperfine interaction with unpaired 4*f* electrons [20]. In 1968, Kuznietz reported ^{14}N spectra from ThN (upfield shift) and UN (downfield shift) [21, 22]. In 2017, a static Fourier transform ^{14}N NMR spectrum of antiperovskite nitride Cr_3GeN recorded at 4.2 K was reported revealing a ^{14}N quadrupolar coupling constant C_Q = 0.3 MHz and a downfield shift [23].

Open Access. © 2021 Zili Ma et al., published by De Gruyter. This work is licensed under the Creative Commons Attribution 4.0 International License.

Despite 99.6% natural abundance of the ^{14}N isotope, solid-state ^{14}N NMR studies of nitrogen-containing materials have rarely been reported. This is due to the spin $I = 1$ and a considerable nuclear quadrupole moment of ^{14}N, which result in signals that are severely broadened by quadrupolar interaction. However, as revealed by recent studies on diamagnetic Ta- and Nb-based oxynitrides and N-doped $BaTiO_3$, ^{14}N MAS NMR spectra of these materials exhibit a single resonance without spinning sidebands, implying that quadrupolar interaction vanishes due to the high local symmetry of N^{3-} moieties [8, 10, 24, 25]. This would only be expected for those with cubic crystal systems ($BaNbO_2N$, $BaTaO_2N$, $BaTi(O,N)_3$; $Pm\bar{3}m$ space group) [24, 26], where the nitrogen anions occupy sites with octahedral symmetry (O_h). Nevertheless, although most of these oxynitride perovskites according to diffraction data develop space groups with lower than cubic symmetry, the appearance of ^{14}N MAS NMR spectra is essentially the same for all. This indicates that the local environments of nitrogen must be almost identical and that there are substantial deviations between the real local and averaged structures [25]. Fortuitous cancellation effects can also occur, in analogy to those that seem to be the case for ZnO (^{67}Zn C_Q = 2.40 MHz) and ZnS (^{67}Zn C_Q = 0.01 MHz), both having the same hexagonal (wurtzite) structure [27, 28].

For paramagnetic systems, the total NMR shift can be expressed as

$$\delta = \delta_{orb} + \delta_{con} + \delta_{pc} \quad (1)$$

where the δ_{orb} term corresponds to the orbital "chemical" shift, the sole shift contribution in diamagnetic systems, whereas the latter two terms arise due to the presence of unpaired electrons. The δ_{con} is associated with the electron-nucleus hyperfine coupling constant (HFCC) and denotes the effect of through-bond polarization called "contact shift", which is operative in close vicinity to paramagnetic ion. The δ_{pc} term called "pseudocontact shift" (PCS) originates from electron-nucleus dipolar coupling and magnetic anisotropy of a paramagnetic center and is long range in nature (r^{-3}). Paramagnetic lanthanide (Ln) ions can induce PCS effects for NMR-active nuclei at distances as long as 25–40 Å [29], which is exploited in biomolecular NMR to study large molecular systems [30–32]. On the other hand, solid-state NMR studies of materials incorporating paramagnetic lanthanide ions are scarce. At short distances between the nuclei of NMR interest and paramagnetic Ln^{3+} ions in solids, both contact and pseudocontact mechanisms contribute to the NMR shift, which complicates data interpretation. ^{89}Y MAS NMR studies of Ln-substituted yttrium pyrochlores $Y_{2-x}Ln_xSn_2O_7$ and $Y_{2-x}Ln_xTi_2O_7$ revealed significant induced paramagnetic shifts of the ^{89}Y NMR signals [33]. Similar effects were observed for ^{27}Al resonances upon incorporation of Ce (or other paramagnetic lanthanides) in $Y_3Al_5O_{12}$ (YAG) [34–36], as well as for ^{43}Ca and ^{45}Sc NMR signals from $CaSc_2O_4$ doped with Ce [37]. However, an understanding of the δ_{con}/δ_{pc} contributions could not be established. ^{17}O MAS NMR studies of paramagnetic lanthanide oxides Ln_2O_3 revealed substantial ^{17}O shifts (hundreds to thousands ppm), with contributions from all three terms: δ_{orb}, δ_{con}, and δ_{pc} [38, 39]. In this work, we explore corresponding effects for nitrogen with ^{14}N MAS NMR on $LaTiO_2N$ and $CeTiO_2N$.

2 Results and discussion

Let us first consider the ^{1}H MAS NMR spectrum of the $LaTiO_2N$ surface (Figure 1a, black trace). The proton signal at 4.9 ppm corresponds to physisorbed H_2O, whereas the remaining resonances originate from different types of bridging (>OH_B) and terminal hydroxyl groups (–OH_T). In contrast, surface proton signals from paramagnetic $CeTiO_2N$ (Figure 1a, red trace) are strongly affected by the presence of unpaired electrons of Ce^{3+} ions and paramagnetic NMR interactions arising thereof [32].

The ^{14}N MAS NMR spectrum of $LaTiO_2N$ is shown in Figure 1b, black trace. The narrow signal at 270 ppm is consistent with the data reported for other diamagnetic oxynitride perovskites that are collected in Table 1. The ^{14}N MAS NMR spectrum of paramagnetic $CeTiO_2N$ is presented in Figure 1b, red trace. Despite being broader and slightly less symmetric, the ^{14}N signal from $CeTiO_2N$ exhibits no induced paramagnetic shift due to unpaired 4*f* electrons when compared to its $LaTiO_2N$ counterpart and other diamagnetic oxynitride perovskites in Table 1. This is remarkable given the direct Ce–N contacts in the network and strong paramagnetic effects observed for surface protons (Figure 1a). This counterintuitive result could be explained by the cancellation of orbital and paramagnetic shift contributions with opposite signs, as it is partially the case for ^{17}O NMR shifts in Sm_2O_3 [39]. However, based on the ^{14}N NMR data in Table 1 for 10 diamagnetic oxynitride perovskites incorporating a variety of metal ions, it is safe to assume that δ_{orb} does not change for $CeTiO_2N$ as well, so the induced paramagnetic shift has to be zero, or δ_{con} and δ_{pc} have to cancel each other out.

To explore these scenarios, the induced paramagnetic ^{14}N NMR shifts were evaluated in terms of electron paramagnetic resonance (EPR) parameters by applying the formalism of Moon and Patchkovskii [42] and Vaara [43–48] to the cluster model derived from the $CeTiO_2N$

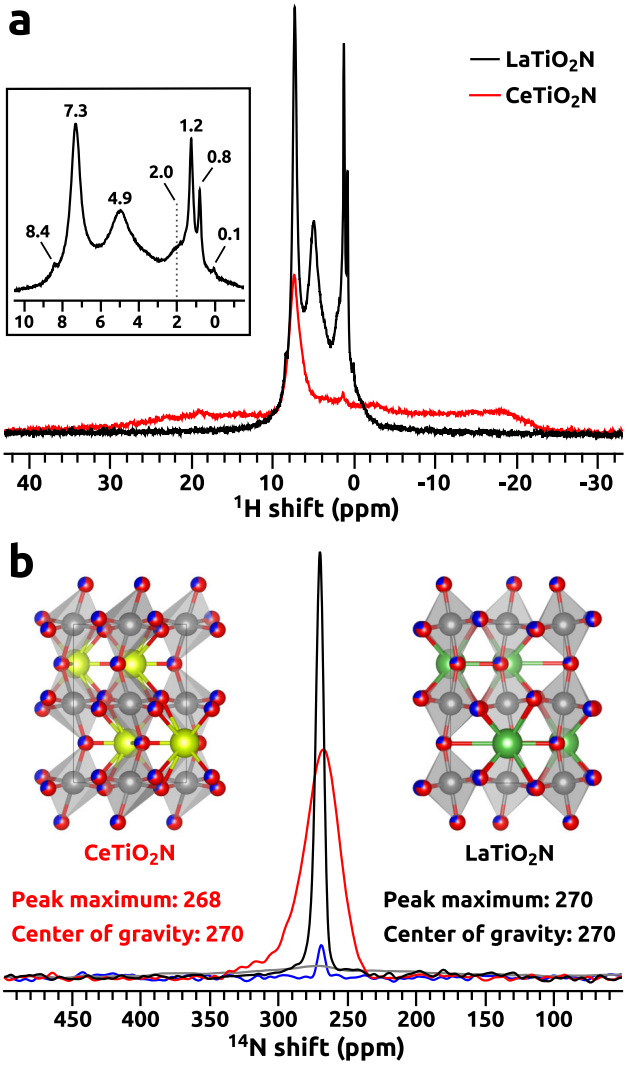

Figure 1: ^{1}H (a) and ^{14}N (b) MAS NMR spectra of $LaTiO_2N$ (black traces), $CeTiO_2N$ (red traces), $NdTiO_2N$ (gray; panel b), and $SrWO_2N$ (blue; panel b) collected at 14.1 T and 60 kHz MAS rate (spectrum of $SrWO_2N$ collected at 43 kHz MAS due to problems with sample spinning). Inset in panel (a) shows zoomed ^{1}H NMR signals from $LaTiO_2N$. Insets in panel (b) display crystal unit cells of both materials (data from refs. [14, 15]) with Ce atoms as yellow, La as green, Ti gray, and O/N red/blue.

crystal lattice. The calculations of ^{14}N hyperfine coupling tensors and the electronic *g*-tensor of Ce were performed with *ab initio* quantum chemistry methods: domain-based local pair natural orbital coupled cluster singlets and doublets (DLPNO-CCSD) [49] and multireference perturbation theory (CASSCF/NEVPT2) [50], respectively. Although this theoretical approach employed an approximation of the averaged structure derived from diffraction measurements, the molecular orbital theory is helpful because it provides an upper/lower boundary of the range of ^{14}N HFCCs expected at the Ce–N distances representative

Table 1: ^{14}N NMR shifts in oxynitride perovskites.

Formula	Space group	^{14}N shift (ppm)
$CaNbO_2N$	*Pnma* [26]	270 [8]
$SrNbO_2N$	*I*4/*mcm* [26]	271 [8]
$BaNbO_2N$	*Pm*$\bar{3}$*m* [26]	270 [8]
$LaNbON_2$	*Pnma* [40]	271 [8]
$CaTaO_2N$	*Pnma* [26]	270–271 [8, 10, 25]
$SrTaO_2N$	*I*4/*mcm* [26]	271–272 [8, 25]
$BaTaO_2N$	*Pm*$\bar{3}$*m* [26]	269–270 [8, 24, 25]
$BaTi(O,N)_3$	*Pm*$\bar{3}$*m* [24]	271 [24]
$LaTaON_2$	*Imma* [17]	270 [8]
$LaTiO_2N$	*Imma* [15]	270 (this work)
$CeTiO_2N$	*Pnma* [14]	268 (this work)
$SrWO_2N$	*Pm*$\bar{3}$*m* [41]	269 (this work)

for the $CeTiO_2N$ crystal lattice and insight into relative magnitudes of contact and PCS contributions. The *ab initio* approach proposed herein for paramagnetic NMR shifts prediction constitutes a potent addition to recent applications of post-Hartree-Fock methods for the NMR shift calculations in diamagnetic systems, providing accuracy beyond standard density functional theory (DFT) (see the SI) [49, 51–54].

The predicted ^{14}N HFCCs for nitrogen positions at the distances of 2.1 and 2.5 Å from Ce in the $CeTiO_2N$ model are −2.0 and −0.9 MHz, respectively (see Table S5 and negative spin densities on nitrogen in Figure 2). These values are in the same range as the experimental estimates of −2.2 and −0.6 MHz for ^{17}O HFCCs in cubic Eu_2O_3 and Sm_2O_3 (Ln–O distances of 2.3–2.4 Å) [39] and the older experimental value of −2.7 MHz estimated for ^{17}O HFCC in the series of paramagnetic lanthanide oxides (Ln_2O_3) [38]. For nitrogen positions at distances ⩾3.3 Å from Ce, predicted magnitudes of ^{14}N HFCCs are <0.05 MHz. Anyway, the scenario that nitrogen atoms experience only distances ⩾3.3 Å from Ce is unrealistic, considering the $CeTiO_2N$ crystal structure.

The calculated induced ^{14}N paramagnetic contact shifts for nitrogen atoms at the distances of 2.1 and 2.5 Å from Ce^{3+} ions are −498 and −213 ppm, respectively (Table S8 in the SI), whereas magnitudes of pseudocontact shifts are <30 ppm and diminish to <10 ppm already at distances ⩾3.3 Å. Therefore, long-range effects from distant paramagnetic centers are unlikely to counteract substantial contact shifts of close Ce–N contacts, given that the next nearest Ce neighbors are >4.5 Å away.

However, as can be seen in Figure 2a, the negative spin density region is associated with the 3*d*-orbital of one of the Ti atoms, in contrast to the mostly positive region observed

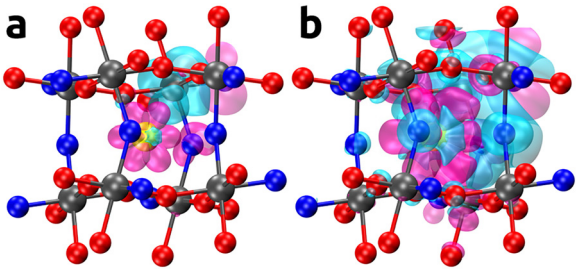

Figure 2: Spin density calculated for the embedded cluster model of $CeTiO_2N$ at the DLPNO-CCSD level of theory shown with isodensity of 0.0025 (a) and 0.00015 *e* bohr^{-3} (b); magenta and cyan denote the positive and negative regions, respectively.

on the Ce 4*f*-orbital. This indicates that the nitrogen atom involved in the bond to this particular titanium atom (site N_2 in the model; Figure S7) may experience cancellation effects of the two. Noteworthily, the calculated induced paramagnetic shift (δ_{con} + δ_{pc}) for site N_2 (see Table S8) of –1.4 ppm (without effects of other Ce^{3+} centers) is close to the experimental paramagnetic shift of –2 ppm (peak maximum). This cancellation effect of spin densities associated with Ce 4*f* and Ti 3*d* orbitals under some particular Ce–N–Ti occupational arrangement could potentially also explain why there is no paramagnetic ^{14}N NMR shift in $CeTiO_2N$ compared with paramagnetic rare-earth nitrides.

To shed light on local symmetry effects, the ^{14}N MAS NMR spectrum of $NdTiO_2N$ was collected. $NdTiO_2N$ is not fully stoichiometric (predicted composition of $NdTiO_{2.17}N_{0.83}$) and exhibits statistical anion distribution resulting in O/N occupational disorder in contrast to other perovskite oxynitrides [55–57]. Therefore, the high local symmetry of nitrogen environments in these systems is not expected to be fully satisfied in $NdTiO_2N$. And this is the case, as the ^{14}N MAS NMR signal of $NdTiO_2N$ was broadened (nearly) beyond detection (Figure 1b, gray trace), which we attribute to occupational disorder combined with paramagnetic effects. This suggests that both the precise O/N settlement in the lattice and its arrangement with respect to Ce and Ti are the origin of the unexpected ^{14}N MAS NMR spectrum of $CeTiO_2N$.

To inspect for the presence of potential impurities occurring in the $CeTiO_2N$ sample, transmission electron microscopy was employed. We could not discern the existence of any additional phases and the selected area electron diffraction pattern was identified to belong to $CeTiO_2N$ and to be consistent with powder X-ray diffraction patterns (see Figure S4 in the SI). Noteworthily, titanium nitride exhibits an approximately 90 ppm higher ^{14}N NMR shift compared with those observed herein [28, 58, 59]. Moreover, to test the hypothesis of amorphous TiO_x/N_y impurities, X-ray photoelectron spectroscopy (XPS) analyses were performed for $LaTiO_2N$ and $CeTiO_2N$ samples, as well as for the reference amorphous TiO_x/N_y film prepared by atomic layer deposition [60]. The latter thin film was obtained by depositing first an amorphous TiO_x layer, followed by ammonolysis at 623 K. These reaction conditions are known to provide amorphous TiO_x/N_y layers. The XPS characteristics of the amorphous TiO_x/N_y reference film are clearly distinct from those of $LaTiO_2N$ and $CeTiO_2N$ (see Figure S5). This indicates that the collected ^{14}N MAS NMR signals do not originate from a potential amorphous side phase TiO_x/N_y.

In addition, we have synthesized $SrWO_2N$ and recorded its ^{14}N MAS NMR spectrum. $SrWO_2N$ has a cubic structure ($Pm\bar{3}m$; Table 1) with tungsten ions being in the $5d^1$ electron configuration [61] and exhibits metallic character, which makes it challenging for MAS NMR. The sharp ^{14}N NMR signal (Figure 1b; blue trace) is consistent with the octahedral symmetry of the nitrogen ions in the structure. The ^{14}N shift of 269 ppm is basically the same as for the 10 diamagnetic oxynitrides presented in Table 1. This renders the ^{14}N shift unsusceptible to the type, oxidation state, and electronic configuration of the cations present in these structures. It is worth noting that hexagonal phases of ZrN, InN, and GaN metal nitrides exhibit similar shifts [59].

3 Conclusions

To conclude, no paramagnetic ^{14}N NMR shift was observed for $CeTiO_2N$ with respect to $LaTiO_2N$ and other diamagnetic oxynitride perovskites. This constitutes the first high-resolution ^{14}N MAS NMR spectrum collected from paramagnetic solid material. *Ab initio* calculations predict ^{14}N hyperfine coupling constants to be similar to those estimated for oxygen in lanthanide oxides by ^{17}O MAS NMR experiments, where effects due to paramagnetic Ln^{3+} ions are substantial. Whereas the invariance of the ^{14}N chemical shift in diamagnetic oxynitrides to the type and oxidation state of the cations involved is quite odd, the absence of any NMR effect either from 4*f* or from 5*d* electrons in $CeTiO_2N$ and $SrWO_2N$ is truly remarkable. Since these features cannot be captured in diffraction-derived, averaged crystal structures, more work is needed to gain insight into local environments in these *unconventional* materials.

4 Experimental section

Solid-state ^{1}H and ^{14}N MAS NMR spectra were acquired at a magnetic field strength of 14.1 T (Larmor frequencies of 600.1 and 43.4 MHz,

respectively) with a Bruker Avance III spectrometer equipped with a 1.3 mm MAS probehead and employing a MAS rate of 60.00 kHz (43.00 kHz for $SrWO_2N$ due to its metallic character and difficulties with sample spinning). ^{1}H NMR acquisitions were performed with a rotor-synchronized, double-adiabatic spin-echo sequence with a 90° excitation pulse of 1.1 μs, followed by two 50.0 μs tanh/tan short high-power adiabatic pulses [62, 63] with a 5 MHz frequency sweep. All pulses operated at a nutation frequency of 210 kHz. 256 signal transients with a 5 s relaxation delay were accumulated. ^{14}N MAS NMR spectra were collected using a 3.0 μs 90° excitation pulse and 65,536 scans collected per sample using a 1 s relaxation delay. The spectrum of $SrWO_2N$ was recorded with the Hahn-echo sequence. ^{1}H shifts were referenced to neat tetramethylsilane (TMS) at 0 ppm, whereas ^{14}N shifts to solid NH_4Cl at 0 ppm (−342.4 ppm with respect to nitromethane).

5 Supporting information

Synthesis and characterization of $LaTiO_2N$, $CeTiO_2N$, and $SrWO_2N$; *ab initio* prediction of induced paramagnetic NMR shifts; computational details and benchmarks are given as Supporting Information available online (https://doi.org/10.1515/znb-2021-0031).

Author contributions: All the authors have accepted responsibility for the entire content of this submitted manuscript and approved submission.
Research funding: None declared.
Conflict of interest statement: The authors declare no conflicts of interest regarding this article.

References

1. Kudo A., Miseki Y. *Chem. Soc. Rev.* 2009, *38*, 253–278.
2. Yerga R. M. N., Galván M. C. A., del Valle F., de la Mano J. A. V., Fierro J. L. G. *ChemSusChem* 2009, *2*, 471–485.
3. Zhang F., Yamakata A., Maeda K., Moriya Y., Takata T., Kubota J., Teshima K., Oishi S., Domen K. *J. Am. Chem. Soc.* 2012, *134*, 8348–8351.
4. Tong H., Ouyang S., Bi Y., Umezawa N., Oshikiri M., Ye J. *Adv. Mater.* 2012, *24*, 229–251.
5. Hisatomi T., Katayama C., Moriya Y., Minegishi T., Katayama M., Nishiyama H., Yamada T., Domen K. *Energy Environ. Sci.* 2013, *6*, 3595–3599.
6. Matsukawa M., Ishikawa R., Hisatomi T., Moriya Y., Shibata N., Kubota J., Ikuhara Y., Domen K. *Nano Lett.* 2014, *14*, 1038–1041.
7. Akiyama S., Nakabayashi M., Shibata N., Minegishi T., Asakura Y., Abdulla-Al-Mamun M., Hisatomi T., Nishiyama H., Katayama M., Yamada T., Domen K. *Small* 2016, *12*, 5468–5476.
8. Cordes N., Bräuniger T., Schnick W. *Eur. J. Inorg. Chem.* 2018, 5019–5026.
9. Ma Z., Thersleff T., Görne A. L., Cordes N., Liu Y., Jakobi S., Rokicińska A., Schichtl Z. G., Coridan R. H., Kuśtrowski P., Schnick W., Dronskowski R., Slabon A. *ACS Appl. Mater. Interfaces* 2019, *11*, 19077–19086.
10. Ma Z., Jaworski A., George J., Rokicińska A., Thersleff T., Budnyak T. M., Hautier G., Pell A. J., Dronskowski R., Kuśtrowski P., Slabon A. *J. Phys. Chem. C* 2020, *124*, 152–160.
11. Grins J., Svensson G. *Mater. Res. Bull.* 1994, *29*, 801–809.
12. Fuertes A. *Dalton Trans.* 2010, *39*, 5942–5948.
13. Yang M., Oró-Solé J., Rodgers J. A., Jorge A. B., Fuertes A., Attfield J. P. *Nat. Chem.* 2011, *3*, 47–52.
14. Porter S. H., Huang Z., Cheng Z., Avdeev M., Chen Z., Dou S., Woodward P. M. *J. Solid State Chem.* 2015, *226*, 279–285.
15. Habu D., Masubuchi Y., Torii S., Kamiyama T., Kikkawa S. *J. Solid State Chem.* 2016, *237*, 254–257.
16. Wolff H., Dronskowski R. *J. Comput. Chem.* 2008, *29*, 2260–2267.
17. Porter S. H., Huang Z., Woodward P. M. *Cryst. Growth Des.* 2014, *14*, 117–125.
18. Kubo A., Giorgi G., Yamashita K. *Chem. Mater.* 2017, *29*, 539–545.
19. Xu X., Jiang H. *RSC Adv.* 2020, *10*, 24410–24418.
20. Shulman R. G., Wyluda B. J. *J. Phys. Chem. Solids* 1962, *23*, 166.
21. Kuznietz M. *J. Chem. Phys.* 1968, *49*, 3731–3732.
22. Kuznietz M. *Phys. Rev.* 1969, *180*, 476–481.
23. Takao K., Liu Z., Uji K., Waki T., Tabata Y., Watanabe I., Nakamura H. *J. Phys.: Conf. Ser.* 2017, *868*, 012021.
24. Bräuniger T., Müller T., Pampel A., Abicht H. P. *Chem. Mater.* 2005, *17*, 4114–4117.
25. Kim Y., Paik Y. *Solid State Sci.* 2012, *14*, 580–582.
26. Kim Y. I., Woodward P. M., Baba-Kishi K. Z., Tai C. W. *Chem. Mater.* 2004, *16*, 1267–1276.
27. Bastow T. J., Stuart S. N. *Phys. Status Solidi* 1988, *145*, 719–728.
28. Bastow T. J., Massiot D., Coutures J. P. *Solid State Nucl. Magn. Reson.* 1998, *10*, 241–245.
29. Allegrozzi M., Bertini I., Janik M. B. L., Lee Y. M., Liu G., Luchinat C. *J. Am. Chem. Soc.* 2000, *122*, 4154–4161.
30. Bertini I., Luchinat C., Parigi G. *Concepts Magn. Reson.* 2002, *14*, 259–286.
31. Benda L., Mareš J., Ravera E., Parigi G., Luchinat C., Kaupp M., Vaara J. *Angew. Chem. Int. Ed.* 2016, *55*, 14713–14717.
32. Pell A. J., Pintacuda G., Grey C. P. *Prog. Nucl. Magn. Reson. Spectrosc.* 2019, *111*, 1–271.
33. Grey C. P., Smith M. E., Cheetham A. K., Dobson C. M., Dupree R. *J. Am. Chem. Soc.* 1990, *112*, 4670–4675.
34. George N. C., Pell A. J., Dantelle G., Page K., Llobet A., Balasubramanian M., Pintacuda G., Chmelka B. F., Seshadri R. *Chem. Mater.* 2013, *25*, 3979–3995.
35. McCarty R. J., Stebbins J. F. *Solid State Nucl. Magn. Reson.* 2016, *79*, 11–22.
36. Carvalho J. P., Jaworski A., Brady M. J., Pell A. *J. Magn. Reson. Chem.* 2020, 1–16.
37. George N. C., Brgoch J., Pell A. J., Cozzan C., Jaffe A., Dantelle G., Llobet A., Pintacuda G., Seshadri R., Chmelka B. F. *Chem. Mater.* 2017, *29*, 3538–3546.
38. Yang S., Shore J., Oldfield E. *J. Magn. Reson.* 1992, *99*, 408–412.
39. Hope M. A., Halat D. M., Grey C. P. *Solid State Nucl. Magn. Reson.* 2019, *102*, 21–30.
40. Logvinovich D., Ebbinghaus S. G., Reller A., Marozau I., Ferri D., Weidenkaff A. *Z. Anorg. Allg. Chem.* 2010, *636*, 905–912.
41. Fawcett I. D., Ramanujachary K. V., Greenblatt M. *Mater. Res. Bull.* 1997, *32*, 1565–1570.
42. Moon S., Patchkovskii S. *Calculation of NMR and EPR Parameters: Theory and Applications*; Wiley-VCH: Weinheim, 2004.
43. Pennanen T. O., Vaara J. *J. Chem. Phys.* 2005, *123*, 174102.
44. Pennanen T. O., Vaara J. *Phys. Rev. Lett.* 2008, *100*, 133002.

45. Rouf S. A., Mareš J., Vaara J. *J. Chem. Theor. Comput.* 2015, *11*, 1683–1691.
46. Vaara J., Rouf S. A., Mareš J. *J. Chem. Theor. Comput.* 2015, *11*, 4840–4849.
47. Pyykkönen A., Feher R., Köhler F., Vaara J. *Inorg. Chem.* 2020, *59*, 9294–9307.
48. Andersen A. B., Pyykkönen A., Jensen H. J., McKee V., Vaara J., Nielsen U. G. *Phys. Chem. Chem. Phys.* 2020, *22*, 8048–8059.
49. Saitow M., Neese F. *J. Chem. Phys.* 2018, *149*, 034104.
50. Ganyushin D., Neese F. *J. Chem. Phys.* 2013, *138*, 104113.
51. Stoychev G. L., Auer A. A., Neese F. *J. Chem. Theor. Comput.* 2018, *14*, 4756–4771.
52. Rzepka P., Bacsik Z., Pell A. J., Hedin N., Jaworski A. *J. Phys. Chem. C* 2019, *123*, 21497–21503.
53. Witwicki M., Walencik P. K., Jezierska J. *J. Mol. Model.* 2020, *138*, 104113.
54. Dittmer A., Stoychev G. L., Maganas D., Auer A. A., Neese F. *J. Chem. Theor. Comput.* 2020, *16*, 6950–6967.
55. Clarke S. J., Guinot B. P., Michie C. W., Calmont M. J. C., Rosseinsky M. *J. Chem. Mater.* 2002, *14*, 288–294.
56. LeGendre L., Marchand R., Piriou B. *Eur. J. Solid State Inorg. Chem.* 1997, *34*, 973–982.
57. Ma Z., Chen K., Jaworski A., Chen J., Rokicińska A., Kuśtrowski P., Dronskowski R., Slabon A. *Inorg. Chem.* 2021, *60*, 919–929.
58. MacKenzie K. J. D., Meinhold R. H., McGavin D. G., Ripmeester J. A., Moudrakovski I. *Solid State Nucl. Magn. Reson.* 1995, *4*, 193–201.
59. Kempgens P., Britton J. *Magn. Reson. Chem.* 2016, *54*, 371–376.
60. Reed P. J., Mehrabi H., Schichtl Z. G., Coridan R. H. *ACS Appl. Mater. Interfaces* 2018, *10*, 43691–43698.
61. Yashima M., Fumi U., Nakano H., Omoto K., Hester J. R. *J. Phys. Chem. C* 2013, *117*, 18529–18539.
62. Hwang T. L., van Zijl P. C. M., Garwood M. *J. Magn. Reson.* 1998, *133*, 200–203.
63. Kervern G., Pintacuda G., Emsley L. *Chem. Phys. Lett.* 2007, *435*, 157–162.

Supplementary Material: The online version of this article offers supplementary material (https://doi.org/10.1515/znb-2021-0031).